# *Articles*

## Anomalous Electrical Conductivity of Nanosheaves of $CeO_2$

Sangtae Kim,*,† Jong Soo Lee,† Christoph Mitterbauer,† Quentin M. Ramasse,‡ Michael C. Sarahan,† Nigel D. Browning,†,§ and Hee Jung Park†

*Department of Chemical Engineering and Materials Science, University of California, Davis, California 95616, National Center for Electron Microscopy, Lawrence Berkeley National Laboratory, Berkeley, California 94720, and Physical and Life Sciences Directorate, Lawrence Livermore National Laboratory, Livermore, California 94550*

*Received June 11, 2008. Revised Manuscript Received February 16, 2009*

$CeO_2$ is a functional oxide known to conduct oxygen ions at elevated temperatures. Enhancement of the ionic conductivity can lead to its application as an electrolyte for solid oxide fuel cells that can operate at low temperatures. We report here a one-dimensional $CeO_2$ nanostructure with a novel sheaflike morphology which exhibits the oxygen-ionic conductivity distinctively higher than that of conventional $CeO_2$ electrolyte. The oxygen nonstoichiometry in the $CeO_2$ nanowires constituting the sheaf was determined by electron energy loss spectroscopy (EELS) and was found to be very small. We thus attribute this anomalously high ionic conductivity to enhanced oxygen-ion mobility at the interfaces between $CeO_2$ nanowires in the sheaf rather than to increased charge-carrier concentration which is often responsible for enhanced ionic conductivity in nanostructured ionic conductors.

### Introduction

Oxide-based nanoscale crystals have been the focus of recent research because of their potential as key constituents for future nanoscale devices in the areas of electronics, optics, catalysis, and mechanical and biomedical applications.[1] The synthesis and physicochemical characteristics induced from their dimensionality and size reduction are the important factors controlling their technological applications.

$CeO_2$ is a fluorite-structured rare earth oxide that exhibits a structural tolerance to reduction that is greater than other oxide systems—allowing a higher concentration of mobile oxygen vacancies to be incorporated into the material. It has been used for a wide variety of applications including automobile exhaust catalysts,[2,3] ultraviolet (UV) blockers,[4] and abrasives.[5] In particular, its ability to serve as a fast oxygen-ion conductor has been the center of attention for decades for use as a solid electrolyte (SE) in solid oxide fuel cells (SOFCs) that may be able to operate at low temperatures—conventional SOFCs employing doped zirconium oxide as the SE[6,7] operate above 800 °C. Currently, it is this high operation temperature for SOFCs that presents material degradation problems, as well as other technological complications and economic obstacles,[7] and limits the full development of these environmentally benign high-efficiency electrical power-generating systems.

One avenue of research that has been extensively pursued in recent years has been the synthesis/fabrication of nanostructures of $CeO_2$ that conceivably can exhibit enhanced oxygen-ionic conductivity[8−10] at lower temperatures. Such an expectation is based on the hypothesis that the oxygen-ion transport via large surface/interface areas in the nanostructure is more favorable than that through the crystal interior. To date, the electrical characteristics of nanostructured $CeO_2$ have been reported almost exclusively for polycrystalline bulk ceramics with nanoscale crystallites (<50 nm)[8,9] and thin films.[10] For these types of samples, the expected enhanced oxygen-ionic conductivity has not been observed.

Unlike other functional oxides, far less attention has been paid to the electrical properties of one-dimensional (1-D) $CeO_2$, such as nanowires. In fact, although 1-D structures can serve as ideal model systems to explore size effects on the electrical conductivity, the electrical conductivity of $CeO_2$ nanowires has never been reported. In this report, we present the synthesis and electrical characterization of unprecedented

* Corresponding author. E-mail: chmkim@ucdavis.edu.
† University of California, Davis.
‡ Lawrence Berkeley National Laboratory.
§ Lawrence Livermore National Laboratory.

(1) Yin, Y.; Alivisatos, A. P. *Nature* **2005**, *437*, 664.
(2) Rodriguez, J. A.; Ma, S.; Liu, P.; Hrbek, J.; Evans, J.; Pérez, M. *Science* **2007**, *318*, 1757.
(3) Trovarelli, A. *Catal. Rev.-Sci. Eng.* **1996**, *38*, 493.
(4) Tsunekawa, S.; Fukuda, T.; Kasuya, A. *J. Appl. Phys.* **2000**, *87*, 1318.
(5) Feng, X.; Sayle, D. C.; Wang, Z. L.; Paras, M. S.; Santora, B.; Sutorik, A. C.; Sayle, T. X. T.; Yang, Y.; Ding, Y.; Wang, X.; Her, Y. S. *Science* **2006**, *312*, 1504.
(6) Steele, B. C. H. *Soild State Ionics* **2000**, *129*, 95.
(7) Steele, B. C. H.; Heinzel, A. *Nature* **2001**, *414*, 345.
(8) Chiang, Y. M.; Lavik, E. B.; Kosacki, I.; Tuller, H. T.; Ying, J. Y. *Appl. Phys. Lett.* **1996**, *69*, 8.
(9) Andersson, D. A.; Simik, S. I.; Skorodumova, N. V.; Abrikosov, I. A.; Johansson, B. *PNAS* **2006**, *103*, 3518.
(10) Kim, S.; Maier, J. *J. Electrochem. Soc.* **2002**, *149*, J73–J83.

10.1021/cm801584e CCC: $40.75 
Published on Web 03/23/2009

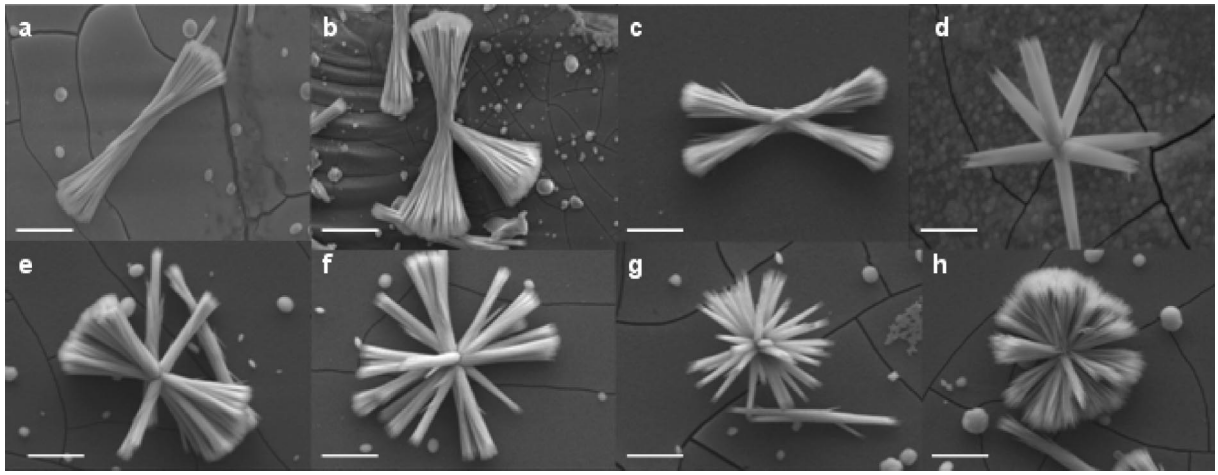


**Figure 1.** Representative SEM images of the nanostructures constituted by $CeO_2$ nanowires. The individual nanowires are about 10 nm thick and over 15 $\mu$m long. The scale bars represent 5 $\mu$m.

nanostructures constituted by $CeO_2$ nanowires. We will demonstrate that the oxygen-ionic conductivity measured from a crystal with a sheaflike morphology (hereafter, referred to as the sheaf) is significantly higher than that of bulk $CeO_2$.

## Experimental Section

To synthesize the $CeO_2$ nanostructures, 0.01 M cerium nitrate ($Ce(NO_2)_3 \cdot 6H_2O$, Aldrich, 99.99%) and 0.01 M hexamethylenetertramine ($C_6H_{12}N_4$, Aldrich) were dissolved in 50 mL of distilled water. This mixture in a sealed container was heated up to 100 °C for 1 h under vigorous stirring. Silicon(100) substrates cleaned with acetone, methanol, and isopropanol subsequently were put into the reaction mixture and then kept at 100 °C for 1 h. After being cooled to room temperature, the Si(100) substrates were collected, washed with distilled water, and dried at 80 °C for 2 h in a dry oven.

Field-emission scanning electron microscopy (FE-SEM, FEI XL-30 SFEG) and high-resolution (scanning) transmission electron microscopy (HR-(S)TEM) were used to characterize the size, shape, structure, and composition of the $CeO_2$ nanostructures with different morphologies that were formed on the Si substrates. Those nanostructures were found to coexist on the Si substrates. To study the electrical properties of the $CeO_2$ nanosheaves, the device was fabricated using a conventional photolithography process. Source and drain Ti/Pt (350/150 nm) electrodes were lithographically patterned on the individual $CeO_2$ nanosheaves dispersed on 100-nm-thick $Si_3N_4$ layer on heavily doped Si substrates. Spacing between the source and drain electrodes was typically 4 $\mu$m. We measured ac impedance spectra of $CeO_2$ nanosheaves using a Novocontrol-Alpha-N frequency analyzer in the frequency range of 10 MHz to 0.1 Hz with an ac amplitude of 30 mV. The measured impedance spectra were fitted using Zview software to estimate the resistance. The dc resistance of the sheaves was measured using a Keithley 236 sourcemeter.

## Results and Discussion

Figure 1 shows representative SEM images of the assorted $CeO_2$ nanostructures synthesized by this method. As indicated in Figure 1, the sheaf (Figure 1a) of $CeO_2$ nanowires, being about 20 $\mu$m long and less than 10 nm thick, initially grows and develops to form the structure with a "pom-pom-ball"-like morphology (Figure 1h). The sheaf and its evolution into complex nanostructures have not previously been reported for any oxide systems.

Recently, $Bi_2S_3$, a main group metal chalcogenide, showed very similar crystal developments to what we observed for our $CeO_2$, although the size of the $CeO_2$ nanostructures is larger by a factor of ~30 than that of the $Bi_2S_3$ structures.[11] Tang and Alivisatos proposed a splitting growth mechanism to explain the growth of $Bi_2S_3$, which resembles the growth of some minerals in nature.[11] The sequential images of splitting shown in Figure 1 indeed suggest that the splitting mechanism can possibly explain the crystal developments in our $CeO_2$ nanostructures. On the other hand, the constituting individual $CeO_2$ nanowires shown in Figure 1 are found to be in polycrystalline forms, although the grain boundary angle is very low (see the TEM analysis on the nanowire discussed below), while the nanostructures of $Bi_2S_3$ reported are constituted by single-crystal $Bi_2S_3$ nanowires.

We measured the electrical resistance of the sheaf using both two-probe ac and dc techniques to investigate the electrical characteristics of such a bundle of 1-D $CeO_2$ nanostructuctures. The ac impedance measurements allow one to probe local resistance in the sample while the dc technique measures the overall resistance.[12] Figure 2a shows a representative ac impedance spectrum with a largely single semicircular arc measured from the sheaf (with sputtered platinum electrodes (see an inset of Figure 2a). The data collected at lower frequencies appeared to be rather scattered as indicated in Figure 2a. We estimated ac resistance by fitting the spectrum using an equivalent circuit consisting of a resistor and a capacitor in parallel, and we found it to be about 6 k$\Omega$ at 360 °C in $O_2$.

We also measured the resistance of a $Si_3N_4$/Si substrate with exactly the same electrode configurations under the condition where Figure 2a was obtained using the ac and the dc techniques. We found that both the ac and dc resistances of the substrate exceed the upper detection limit of the analyzers (ca. teraohms). We thus concluded that Figure 2a was measured exclusively from the sheaf. Figure

(11) Tang, J.; Alivisatos, A. P. *Nano Lett.* **2006**, *6*, 2701.
(12) Basoukov, E.; Macdonald, J. R. In *Impedance Spectroscopy: Theory, Experiment, and Applications*; Basoukov, E., Macdonald, J. R. Eds.; John Wiley & Sons: New York, 2005.
(13) Kudo, T.; Obayashi, H. *J. Elecrochem. Soc* **1976**, *123*, 415.

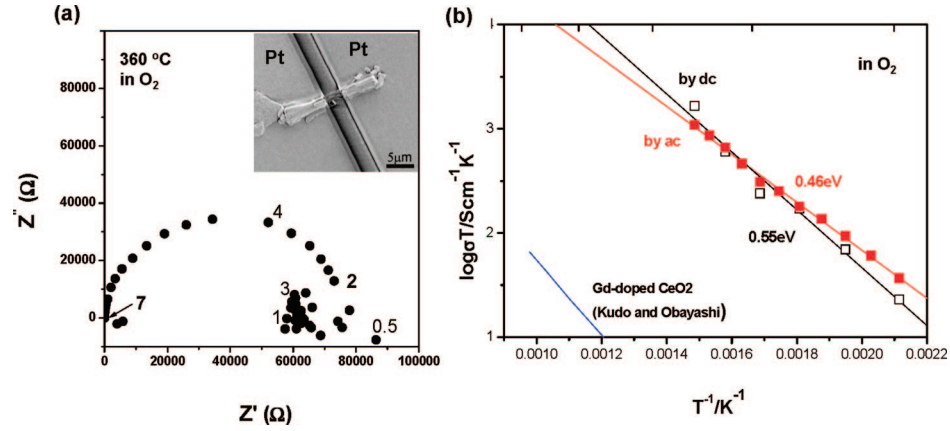


**Figure 2.** Representative impedance spectrum (a Nyquist plot) measured from a device with the sheaf (see the inset) in the frequency range of 10 MHz to 0.1 Hz with an ac amplitude of 30 mV. The frequencies are indicated in a logarithmic scale. (a) An Arrhenius plot of the measured ac (solid squares) and dc (open squares) conductivities (b). Also shown is the oxygen-ionic conductivity reported for 20 mol % Gd-doped $CeO_2$ for comparison.[13]

2a is consistent with impedance spectra with a single arc that have been previously observed for polycrystalline $CeO_2$ ceramics with the grain size below 30 nm.[10]

We then computed the ac conductivity ($\sigma$) that corresponds to the measured ac resistance using the relation $\sigma = l/(RA)$ with $l$ and $A$ being the distance between two electrodes and the cross-sectional area of the middle of the sheaf (i.e., 3 $\mu$m and $\sim$0.8 $\mu m^2$, respectively) that is assumed to be identical to the cross-sectional area multiplied by the number of $CeO_2$ nanowires in the sheaf, respectively (see Figure 1 in the Supporting Information for details). Figure 2b shows Arrhenius behavior of the conductivity. $CeO_2$ conducts electrons as well as oxygen ions. If $CeO_2$ is pure, both the electronic and the ionic conductivities should vary with varying ambient oxygen partial pressure ($P_{O_2}$) at temperatures where gaseous oxygen can incorporate into the material. This is because the number of both ionic and electronic charge carriers (i.e., oxygen vacancies and electrons, respectively) in the material is determined by the red-ox equilibrium reaction (i.e., $O(s) = {}^1/_2O_2(g) + 2e^-(s) + V^{2+}(s)$ where V denotes oxygen vacancy at the solid surface) at the gas−solid interface. On the other hand, in impure (i.e., doped) $CeO_2$, the charge-carrier concentrations are determined by the number of impurities (or dopants). For instance, the number of oxygen vacancies in $CeO_2$ is fixed by impurities if the impurities serve as acceptors (i.e., the impurities with the valence state lower than +4, which is the valence state of Ce). The number of oxygen vacancies created by such acceptor doping (i.e., $c_V = (1/2)c_A$ with $c$ being concentration; subscript "A" denotes acceptor impurities with the valence state of +3) typically far exceeds those produced by the red-ox reaction and thus hardly varies over a wide range of $P_{O_2}$ of the ambient gas. In this regime, $CeO_2$ becomes a predominantly oxygen-ionic conductor. If the valence state of the impurities is higher than +4, the impurities serve as donors to create electrons (by reducing $Ce^{4+}$ to $Ce^{3+}$) in $CeO_2$. We found that the conductivity of the sheaf remained unchanged in the $P_{O_2}$ of $1-10^5$ Pa at 400 °C at which the red-ox kinetics is reasonably fast.[9] The equilibration time under each $P_{O_2}$ was over 24 h. We attribute the observed conductivity invariant with $P_{O_2}$ to extrinsic oxygen-ionic conduction in the sheaf because of the following:

(1) It is reasonable to believe that the valence sate of background impurities typically found in $CeO_2$ is lower than +4 such that the sheaf can hardly be a donor-doped electronic conductor. Indeed, the valence state of Ce in the sheaf is found to be +4 (see the EELS results discussed below), indicating that the electron concentration in the sheaf is minimal.

(2) The activation energy estimated from the Arrhenius plot of the ac conductivity was 0.46 eV as indicated in Figure 2b. This value is consistent with the value reported for the ionic conduction in pure $CeO_2$[9] and slightly lower than the value of $\sim$0.6 eV reported for the ionic conduction in acceptor-doped $CeO_2$.[10] (The activation energies of the electronic conductivities measured from various donor-doped (<5 mol %) $CeO_2$ range from 0.29 to 0.36 eV[14−16]).

(3) We also estimated dc conductivity of the sheaf and found that the dc conductivity was lower than the corresponding ac conductivity at lower temperatures as shown in Figure 2b. The dc and ac conductivities, however, became nearly identical to one another at higher temperatures.

Note that, as mentioned above, the dc resistance includes the resistance not only in the $CeO_2$ nanosheaf but also at the electrode while the ac resistance, that is, the resistance we estimated by fitting a large semicircular arc that appeared in the Nyquist plot such as the one shown in Figure 2b, represents the resistance only in the sheaf. The electrode resistance can be attributed to the slower red-ox kinetics at the gas−solid interface at lower temperatures which becomes insignificant at higher temperatures. This result is also consistent with the fact that the conduction in the sheaf is due to oxygen transport.

We notice from Figure 2b that the absolute values of the conductivity of the sheaf is over 2 orders of magnitude higher

(14) De Guire, M. R.; Shingler, M. J.; Dincer, E. *Solid State Ionics* **1992**, *52*, 155.
(15) Stratton, T. G.; Tuller, H. L. *J. Chem. Soc., Faraday Trans. 2* **1987**, *83*, 1143.
(16) Yashiro, K.; Suzuki, T.; Kaimai, A.; Matsumoto, H.; Nigara, Y.; Kawada, T.; Mizusaki, J.; Sfeir, J.; Van herle, J. *Solid State Ionics* **2004**, *175*, 341.

than that of bulk ceria doped with 20 mol % Gd (CGO-20). CGO-20 is known to have the highest oxygen-ionic conductivity among acceptor-doped $CeO_2$.[6,13,17] It has been recently reported that fluorite-structured oxygen-ionic conductors show enhanced ionic conductivity under a wet atmosphere at low temperatures (<200 °C) due to the fact that it conducts protons as well as oxygen ions when the grain size becomes very small (below 20 nm).[18,19] To provide verification that such high ionic conductivity of the sheaf measured is exclusively due to oxygen-ionic transport, we also measured the conductivity of the sheaf under water-saturated atmosphere ($P_{H_2O}$= 23000 ppm). However, we found that the conductivity remained constant even under such a wet condition in the temperature range of interest. The conductivity can be overestimated by underestimating the electrode area when it is computed. The area we assumed (see Figure 1 in the Supporting Information) is, however, rather close to the upper limit of the electrode area that can possibly be postulated rather than to the lower limit (i.e., the actual area covered by the Pt electrode on the sheaf). Furthermore, the conductivity enhancement observed is too significant to be attributed merely to uncertainty in the electrode area. We thus conclude that the sheaf has significantly higher oxygen-ionic conductivity compared to bulk $CeO_2$.

The electrical conductivity is determined by both the concentration and the mobility of the charge carriers. We postulate that the observed enhanced oxygen-ionic conductivity of the sheaf is mainly due to the enhanced mobility of the oxygen vacancy rather than its concentration variation at the interface. Such hypothesis is based on the fact that $CeO_2$ nanowires constituting the sheaf are undoped such that the number of oxygen vacancies in the $CeO_2$ nanowires must be pinned only by existing background impurities as mentioned above. However, the measured ionic conductivity of the sheaf is too high to be attributed only to the oxygen nonstoichiometry created by such impurities in the sheaf (see the EELS results discussed below for details). On the other hand, it has been reported for nanocrystalline YSZ bulk ceramics that the oxygen diffusivity in the grain boundary is greater than that in the bulk according to the secondary ion mass spectroscopy (SIMS) analysis,[20] although such a result is still in debate[21] and has not been confirmed by conductivity studies yet. To provide further verification of our postulate, we demonstrate in the following the detailed microstructural and chemical analysis on the sheaf to quantitatively measure the oxygen nonstoichiometry in the sheaf.

Figure 3a shows a secondary electron image of a sheaf on a holey carbon grid and Figure 3b an HR-TEM image of the tip of a single wire. We found that the crystalline $CeO_2$ nanowires are encapsulated in an amorphous matrix. The high-angle annular-dark-field (HAADF) HR-STEM image (see Figure 3b), which was performed on a 100 keV, Nion-Corrected VG STEM (VG),[22] shows the interface between the crystalline and the surrounding amorphous part of one of the $CeO_2$ nanowires. The inspection of several HAADF images, using fast Fourier transform (FFT) analysis, reveal grain boundary angles of 6−7°.

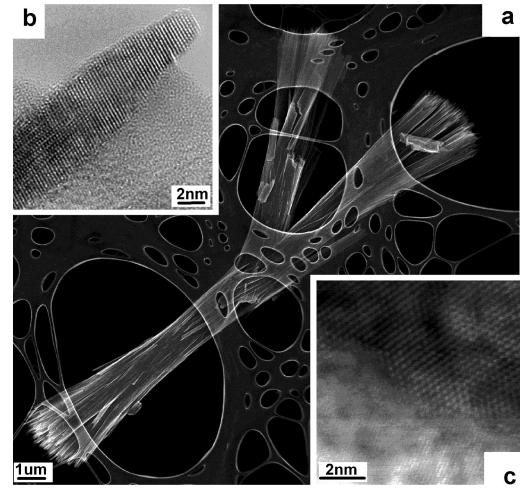


**Figure 3.** (a) Secondary electron (SE) image assembled from two individual SE images showing a sheaf on a holey carbon grid. (b) HR-TEM micrograph of the tip of a single wire. The crystalline wires are surrounded by an amorphous matrix. (c) High-angle annular-dark-field (HAADF) HR-STEM image (VG) showing the interface between the crystalline and the surrounding amorphous part of one of the single wires.

Electron energy loss spectroscopy (EELS) can be used to investigate subtle changes of structure and/or chemical composition changes.[23] Figure 4a shows the HR-TEM image from the region which was used for an EELS line scan (points 1−9) (see Figure 2 in the Supporting Information for details). There is an obvious broadening of the plasmon feature (maximum at ∼27 eV) of the low-loss regions (Figure 4b, Fourier log deconvoluted) between the amorphous (2 + 8) and the crystalline parts (3−7) of the specimen. The inset spectra show the detail in the Ce $M_{4,5}$ edge at ∼110 eV energy loss and show slight variations in the edge intensities as well as in the peak positions. The EELS fine structure (ELNES) of the Ce $M_{4,5}$ ionization edge can be used to identify the oxidation state(s) of Ce. The $M_{4,5}$ edges (Figure 4c) reflect transitions of 3d core electrons to unoccupied states of p- and f-like symmetry. The weak postedge features at ∼890 and 907 eV indicate the presence of $Ce^{4+}$ compounds. The relative quantities of $Ce^{4+}$ and $Ce^{3+}$ were calculated by comparing the relative peak areas of the $M_5$ and $M_4$ edges, according to the calibration data presented by Garvie and Buseck.[24] Peak areas were calculated according to the procedure presented by Wang et al., with the use of a Gaussian fit rather than a Lorentzian, as the former is a built-in function of Digital Micrograph.[25]

The EELS quantification using the M5:M4 ratio gives an approximately constant stoichiometry over the whole region,

(17) Wang, D. Y.; Park, D. S.; Griffith, J.; Nowick, A. S. *Solid State Ionics* **1981**, *2*, 95.
(18) Anselmi-Tamburini, U.; Maglia, F.; Chiodelli, G.; Riello, P.; Bucella, S.; Munir, Z. A. *Appl. Phys. Lett.* **2006**, *89*, 163116.
(19) Kim, S.; Anselmi-Tamburini, U.; Park, H. J.; Martin, M.; Munir, Z. A. *Adv. Mater.* **2008**, *20*, 556.
(20) Knöner, G.; Reimann, K.; Röwer, R.; Södervall, U.; Schaefer, H. E. *PNAS* **2003**, *100*, 3870.
(21) De Souza, R. A.; Pietrowski, M. J.; Anselmi-Tamburini, U.; Kim, S.; Munir, Z. A.; Martin, M. *Phys. Chem. Chem. Phys.* **2008**, *10*, 2067.
(22) Krivanek, O. L. *Ultramicroscopy* **1999**, *78*, 1.
(23) Egerton, R. F. In *Electron Energy-Loss Spectroscopy in the Electron Microscope*, 2nd ed.; Plenum Press: New York, 1996.
(24) Garvie, L. A. J.; Buseck, P. R. *J. Phys. Chem. Solids* **1999**, *60*, 1943.
(25) Wang, F.; Malac, M.; Egerton, R. F. *Micron* **2006**, *37*, 316.

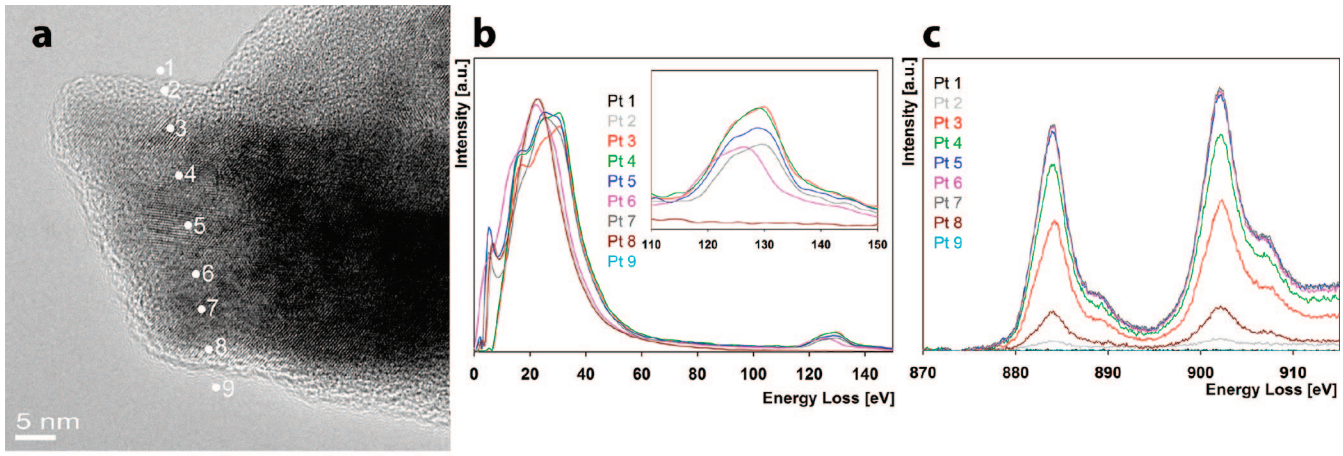


**Figure 4.** (a) HR-TEM image showing the EELS line scan (points 1−9; JEOL). (b) Low-loss spectra. Inset: detail of Ce $M_{4,5}$ low-loss edge at 110 eV. (c) Ce $M_{4,5}$ ionization edges were used for the determination of the quantitative composition.

**Table 1. Quantification of Stoichiometry Using Cerium M5:M4 Edge Ratios**[a]

| sample point | M5:M4 ratio | avg. Ce Ox. state | charge-balanced stoichiometry, CeOx |
|---|---|---|---|
| 3 | 0.683 | 3.99 | 1.99 |
| 4 | 0.674 | 4.03 | 2.01 |
| 5 | 0.670 | 4.05 | 2.02 |
| 6 | 0.675 | 4.02 | 2.01 |
| 7 | 0.668 | 4.03 | 2.01 |
| 8 | 0.674 | 4.03 | 2.01 |

[a] Point 2 was omitted due to inadequate signal.

as seen in Table 1. This is in excellent agreement with the quantification of the energy-dispersive X-ray spectra (EDXS; not shown here) and confirms the very small nonstoichiometry in the sheaf.

Therefore, the quantitative analysis of the oxygen stoichiometry in the sheaf supports the postulation that the observed high oxygen-ionic conductivity is mainly due to enhanced oxygen-ionic mobility rather than increased oxygen vacancy concentration at the interface between $CeO_2$ nanowires.

## Conclusion

Our observation demonstrates abnormally fast oxygen-ionic conduction in a $CeO_2$ nanostructure consisting of polycrystalline 1-D $CeO_2$ nanowires. Previously reported enhanced ionic conductivity in nanostructured ionic solids (e.g., $F^-$ conduction in thin film fluorites) has been shown to be due to enhanced ionic charge-carrier concentration at the interfaces in the materials. [26,27] However, the high oxygen-ionic conductivity that we measured from the $CeO_2$ sheaf is understood by high oxygen ion mobility in this structure since the oxygen nonstoichiometry of the material is very small. We thus speculate that the amorphous layer encapsulating the nanowire may serve as a fast conduction pathway. However, a clear conduction mechanism is not at hand and more work needs to be done to better understand the oxygen ion transport phenomena in such 1-D nanostuctured $CeO_2$. This result deserves further studies on the role of the amorphous layer in the ionic conductivity of the sheaf and theoretical calculations on the ionic diffusion barrier in the amorphous layer. We believe that our unprecedented observation will stimulate both fundamental and practical interest particularly in ion transport phenomena in 1-D nanostructures that leads to development of nanoscale ionic devices.

**Acknowledgment.** J.S.L. is grateful for partial support from the Korea Research Foundation Grant funded by Korea Government for this work (MOEHRD, Basic Research Promotion Fund, KRF-2005-214-D00305). N.D.B. gratefully acknowledges the support from the Department of Energy (DE-FG02-03ER46057).

**Supporting Information Available:** This material is available free of charge via the Internet at http://pubs.acs.org.

CM801584E

(26) Maier, J. *Prog. Solid State. Chem.* **1995**, *23*, 171.
(27) Sata, N.; Eberl, K.; Eberman, K.; Maier, J. *Nature* **2000**, *408*, 946.